Heterogeneity of volatile sources along the Halmahera arc, Indonesia

Bani P.[1], Nauret F.[1], Oppenheimer C.[2], Aiuppa A.[3], Saing B.U.[4], Haerani N.[4], Alfianti H., Marlia M.[4], Tsanev V.[4],

1-Laboratoire Magmas et Volcans, Université Blaise Pascal-CNRS-IRD, OPGC, 63170 Aubière, France

2- Department of Geography, University of Cambridge, Downing Place, Cambridge CB2 3EN, UK

3- Dipartimento DiSTeM, Università di Palermo, 90123 Palermo, Italy

4- Center for Volcanology and Geological Hazard Mitigation (CVGHM), Jl. Diponegoro No. 57, Bandung 40122, Indonesia;

Abstract

The parallel Halmahera and Sangihe arcs in eastern Indonesia are a site of active arc-arc collision of considerable interest in developing understanding of the geodynamics and geochemistry of subduction zones. Owing to the comparative remoteness of the region, rather few ground-based studies of the volcanoes have been undertaken. Here, we report and integrate gas measurements and (isotope) geochemical analyses of lava samples for Dukono, Ibu, Gamkonora, Gamalama, and Makian volcanoes of the Halmahera arc. Summing gas fluxes for all five volcanoes indicates arc-scale emission budgets for H_2O, CO_2, SO_2, H_2S and H_2 of 96300, 2093, 944, 79 and 15 Mg/d, respectively. Dukono is the strongest source of SO_2 and H_2, while Ibu emits the most H_2O and H_2S. Both Gamalama and Ibu are strong CO_2 sources. Volcanic gas CO_2/S_T ratios decrease with distance from the trench, with Dukono (farthest from the trench) emitting the most CO_2-poor gas. Geochemical and isotopic analyses of recent ejecta emphasize the role of high fluid fluxes in the mantle wedge, necessary for partial melting of depleted mantle. Pb, Nd, and Sr isotope ratios, combined with Ba/Nd, Zr/Nd, Ba/Th, and Zr/Nb ratios, evidence compositional variability along the Halmahera arc, and indicate decreasing subducted

sediment contribution from south (Makian, Gamalama) to north (Gamkonora, Ibu, Dukono). Additionally, fluids formed by dehydration of altered oceanic become prominent at the northern volcanoes. We find that the geochemical evolution previously recgonised between Neogene and Quaternary is comparable to the present-day compositional variability we observe along the length of the Halmahera arc.

1. Introduction

The Halmahera arc is situated in the northeastern part of Indonesia and extends in a roughly north-south direction between 3°N-1°S and 127°-128°E. It is the smallest of the four volcanic arcs that constitute the archipelago of Indonesia, with five active volcanoes, namely Dukono, Ibu, Gamkonora, Gamalama, and Makian (also known as Kie besi) from north to south (Fig.1). Due to its comparative remoteness, difficulty of access and political, ethnic and inter-faith unrest that persisted until the early 2000s (Goss, 2000; Bertrand, 2003), the Halmahera arc has been little studied, despite the fact that its volcanoes are among the most active in Indonesia. This picture is starting to be redressed with several recent studies highlighting the strong volcanic degassing source on Dukono (Carn et al., 2017; Bani et al., 2018), the fast-growing rate of Ibu lava dome since 1998 (Agustan et al 2010; Saing et al., 2014), the magmatic signature of weak degassing at Gamkonora (Saing et al., 2020), and the interplay of hydrothermal, magmatic and tectonic processes controlling recurrent eruptive activity of Gamalama volcano (Kunrat et al., 2020). Here, we report the first observations of gas compositions for Ibu volcano that, in combination with recently available data, enable assessment of the arc-scale gas emissions budget. We also highlight the compositional variability of magmas along the arc, based on analyses of recently erupted products.

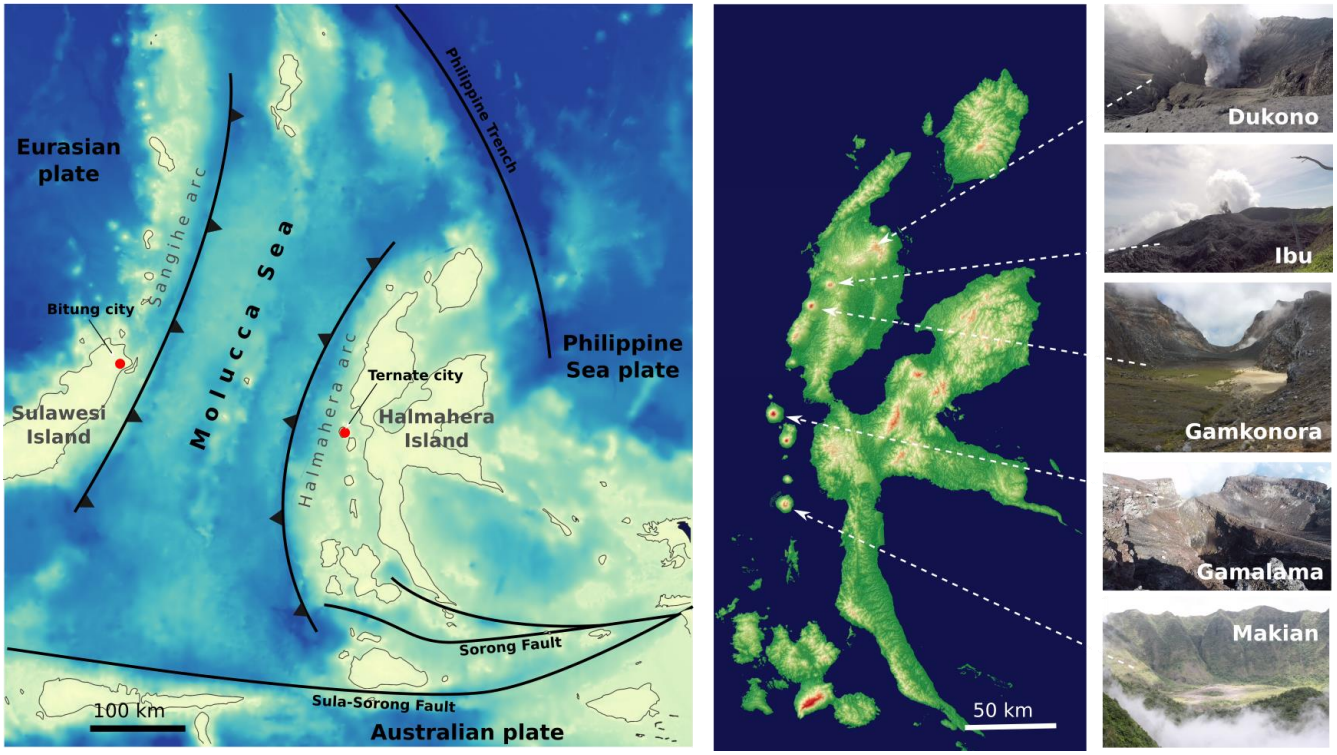

Figure 1. The Halmahera and Sangihe arcs are associated with the double subduction of the Molucca Sea plate. This latter dips west to form the Sangihe arc and east to form the Halmahera arc leading to progressive shrinking of the Molucca Sea. The shortest distance between the two arcs – between Bitung and Ternate is 250 km. The active volcanoes of Halmahera arc, from north to south, are Dukono, Ibu, Gamkonora, Gamalama, and Makian.

2. Geodynamic setting and volcanic activity

The geodynamics of the Halmahera arc are intimately linked to the tectonic activity in the Molucca Sea, where the Sangihe forearc is overriding the Halmahera forearc (e.g., Hall and Wilson, 2000). The process constitutes a unique present-day example of an arc-to-arc collision arising from the double subduction of the Molucca Sea plate, which dips west beneath the Eurasian plate and east under the Philippine Sea plate (Fig.1, Baker et al., 1994; Forde, 1997; Hall and Wilson, 2000; Zhang et al., 2017). Prior to subduction, the Molucca Sea plate stretched ~1000 km between Sulawesi and

Halmahera (Morris et al., 1983). It started to be consumed in the lower Miocene (17 Ma) first to the west to form the Sangihe arc and then to the east within the last 3 Ma to form the Halmahera arc (Hamilton, 1979; Forde, 1997). The two facing arcs are now only 250 km apart at their closest points. According to Baker et al. (1994), in the early Neogene, the Australian continental margin collided with a volcanic arc at the southern limit of the Philippine Sea plate. This collision caused the Philippine Sea plate to rotate clockwise. Subsequently, the former subduction boundary evolved into a major left-lateral strike-slip system – the Sorong fault (Fig.1) – that has displaced the Australian continent fragment and Philippine Sea plate into the Molucca Sea, resulting in subduction of the Molucca Sea plate.

2-1. Dukono

Dukono is one of the most active volcanoes in Indonesia (Bani et al. 2020). It has been continuously erupting since 1933 (GVP, 2013, (Dukono); Bani et al., 2018) but with variable intensity. Since 2006 the volcano has produced intermittent strong ash emissions at variable discharge rates, and heavy ash falls have regularly impacted nearby Tobelo city, 14 km east of the volcano. Dukono has a single ~600 m wide crater hosting up to three active vents . Unlike the other conical volcanoes of the Halmahera arc, Dukono (culminating at 1229 m a.s.l.) is part of a larger volcanic complex (Fig.2). Dukono gas measurements are reported in Bani et al., 2018.

2-2. Ibu

Ibu was quiescent for nearly a century (Saing et al., 2014) until 1998 when a violent, sudden eruption occurred on new year's eve. Since then, the volcano has erupted viscous lava that destroyed dense forest in the crater, and progressively a lava dome built up to and over the crater rim currently extending to the north, and an increasing concern for the local population. Simultaneously, Ibu also exhibits a continuous eruptive activity through its 3 active vents (Fig.2). The first gas measurements were reported provided by Saing et al (2014) who estimated a daily SO_2 release of 1.3 Mg via the

eruptive discharges. Ibu summit crater culminates at 1325 m (a.s.l.) and meter sized ejecta are often thrown beyond the crater rim. These ejecta have been collected and analyzed by Saing et al (2014).

2-3. Gamkonora

The last recorded eruption of Gamkonora was a VEI 2 event on Jan. 4, 2013, that propelled a thick gray ash column up to 2000-2500 m above the summit. The eruptive history of this volcano is described in Saing et al. (2020). Over the last 450 years, Gamkonora experienced 17 eruptions. The largest eruption documented is a VEI 5 event in 1673 (Siebert et al., 2010) that resulted in tsunami that inundated nearby coastal areas (Paris et al., 2014). The summit morphology of Gamkonora is characterized by a large and elongated depression that resulted from successive north-south crater formations. The currently active crater is located towards the southern end of this elongated depression. It hosts an active vent of about 50 m in diameter (Fig.2). The active crater is wide open to the south possibly following a large crater-wall failure.

Access to the summit is challenging and only a few expeditions have been carried out. Gas composition has been previously measured using MultiGAS equipment placed on the summit fracture (Kunrat et al., 2020), whilst SO_2 flux measurements were carried out 4.5 km NW of the summit (Fig.2), on a vertical scanning mode on July 19-21, 2015 (Kunrat et al., 2020) and with an angle of 20° from horizontal on July 8, 2014. Additional measurements were made during Jul. 19-21, 2015 during an eruption (Fig.2). However, as widely recognized (e.g., Andres and Kasgnoc, 1998; Bani et al., 2009), eruptive gas discharges are ephemeral and unrepresentative of a volcano's long-term degassing budget.

2-4. Gamalama

Gamalama is considered one of the most dangerous volcanoes in Indonesia owing to its proximity to the city of Ternate (more than 200,000 inhabitants) and its recurrent eruptive activity (GVP, 2003, Gamalama). Since the first documented eruption in 1510, Gamalama has experienced 67 eruptions. In the last decade, the volcano erupted every 1 or 2 years (GVP, 2003, Gamalama). According to Kunrat et

al. (2020), the frequency of eruptions reflects a combination of magmatic and phreatic processes, enhanced by large fractures under the influence of regional geodynamics. The current degassing occurs through a large NE-SW fracture that transects the summit cone.

2-5. Makian

Makian is the southernmost active volcano of the Halmahera arc and is the least known of the arc. The volcano has eight confirmed eruptions since 1550 (GVP, 2003, Makian), including three of VEI 4 and two of VEI 3. The latest eruption was a VEI3 event in 1988 that prompted the evacuation of 15,000 inhabitants (GVP, 2003, Makian). Since then, the volcano has remained calm.

3. Methodology

3-1. Field measurements

SO_2 flux measurements were made with passive ultraviolet spectrometers that scanned the plume from a fixed position and using the retrieval method of differential optical absorption spectroscopy (DOAS) (Fig.2). Spectra were obtained with a variable step angle, depending on the plume size and distance from the plume. The spectrometer used was an Ocean Optic USB2000+ with a spectral range of 290–440 nm and spectral resolution of 0.5 FWHM. The SO_2 column amounts (ppm m) were retrieved using standard DOAS calibration and analysis procedures (Platt and Stutz 2008). Reference spectra included in the non-linear fit were obtained by convolving high-resolution SO_2 (Bogumil et al. 2003) and O_3 (Voigt et al. 2001) cross-sections with the instrument line shape. A Fraunhofer reference spectrum and Ring spectrum, calculated with the DOASIS program, were included in the fit. The integrated plume SO_2 cross-section was then multiplied by the plume rise speed to derive SO_2 emission rate. Gas compositions were measured using a Multicomponent Gas Analyser System (Multi-GAS; Aiuppa et al., 2005; Shinohara, 2005; Fig.2). This portable instrument measures the abundances of CO_2, SO_2, H_2S, H_2, as well as ambient atmospheric pressure (P), temperature (T), and relative humidity (RH). This latter is converted into plume H_2O concentrations following Buck

(1981). CO_2 is measured with a commercial infrared spectrometer (range 0–3000 ppm) while SO_2, H_2S, H_2 gases were quantified using specific electrochemical sensors (typical range 0–200 ppm).

ADD SAMPLING METHODS

3-2. Laboratory analytical procedure

Major-element concentrations were obtained by ICP-AES after the dissolution of 100 mg of each sample by alkaline fusion. Trace-element contents were measured by ICP-MS after the dissolution of 100 mg of each sample following Barrat et al. (1996). Comparison with repeated analysis of international standards (AVG-2, BIR-1, and BEN) was used to validate major and trace element data. For most of the elements, the precision is better than 5%, except for elements such as Ni, Cr, and Sc (10%). Pb isotopic compositions were measured by MC-ICP-MS following White et al. (2000). Total procedural blanks vary between 0.12 and 0.24 ng of Pb, with an average of 0.15 ng (n=6), which is negligible (0.05%) compared with the amount of Pb loaded on the columns (200 to 500 ng). We used international standards (AGV2, BHVO2, and BIR-1) to test the reproducibility of our method. Values obtained for AGV-2 are $^{206}Pb/^{204}Pb$ = 18.870, $^{207}Pb/^{204}Pb$ = 15.618, $^{208}Pb/^{204}Pb$ = 38.546 (n = 5), for BHVO-2: $^{206}Pb/^{204}Pb$ = 18.608, $^{207}Pb/^{204}Pb$ = 15.536, $^{208}Pb/^{204}Pb$ = 38.212 (n = 2) and for BIR-1: $^{206}Pb/^{204}Pb$ = 18.848, $^{207}Pb/^{204}Pb$ = 15.655, $^{208}Pb/^{204}Pb$ = 38.489 (n = 1). These results are in agreement with the international reference values (AGV-2: 18.859 to 18.879, 15.609 to 15.627, and 38.511 to 38.7127; BHVO-2: 18.514 to 18.687, 15.457 to 15.558 and 38.232 to 38.294, and BIR-1: 18.834 to 18.889, 15.640 to 15.674 and 38.449 to 38.542 for $^{206}Pb/^{204}Pb$, $^{207}Pb/^{204}Pb$, and $^{208}Pb/^{204}Pb$ respectively). All measured Pb isotope compositions were corrected for mass fractionation by adding a solution of the NIST SRM997 Tl standard to the sample before measurement. Finally, data were re-normalized to the values recommended for the NIST SRM 981 (Galer et al., 1998). Strontium isotopic measurements were carried out by thermal ionization mass spectrometry (TIMS, Triton, ThermoScientific) in static mode with relay matrix rotation (virtual amplifier) on single Re filaments.

The samples were leached in 1 ml HCl 1 N for 15 min in an ultrasonic bath, followed by 45 min at 70 °C on a hotplate. After centrifuging, the supernatant was discarded and the residue was digested in 1 ml concentrated HF and 1 ml concentrated HNO_3. Chemical separation of Sr was achieved following Pin et al. (2014). Sr blanks for the complete procedure are below 5 ng. Sr isotopic measurements were corrected for mass-fractionation using an exponential law and $^{86}Sr/^{88}Sr = 0.1194$ and were normalized using the NIST SRM987 standard ($^{87}Sr/^{86}Sr = 0.710245$). Nd isotopic measurements were corrected for mass fractionation using an exponential law and $^{146}Nd/^{144}Nd=0.7219$ and normalized using Jndi-1 Nd standard ($^{143}Nd/^{144}Nd = 0.512100 \pm 5$ (2σ), n = 5). External reproducibility was monitored by repeated analyses of JNdi-1 Nd standard (143Nd/144Nd=0.512097±10 (2σ), n=13). This value is equal, within error margins, to the proposed value for JNdi-1 standard.

3-4. Sampling sites

3-4-1. Dukono

Figure 3 provides the locations of the instruments and the ash-tephra sampling site. The MultiGAS was positioned at the crater rim and in the plume while the Scanning DOAS was performed on a vertical mode beneath the plume downwind (Fig.2). The field sampling and gas measurements were carried out on July 12 and 13, 2015.

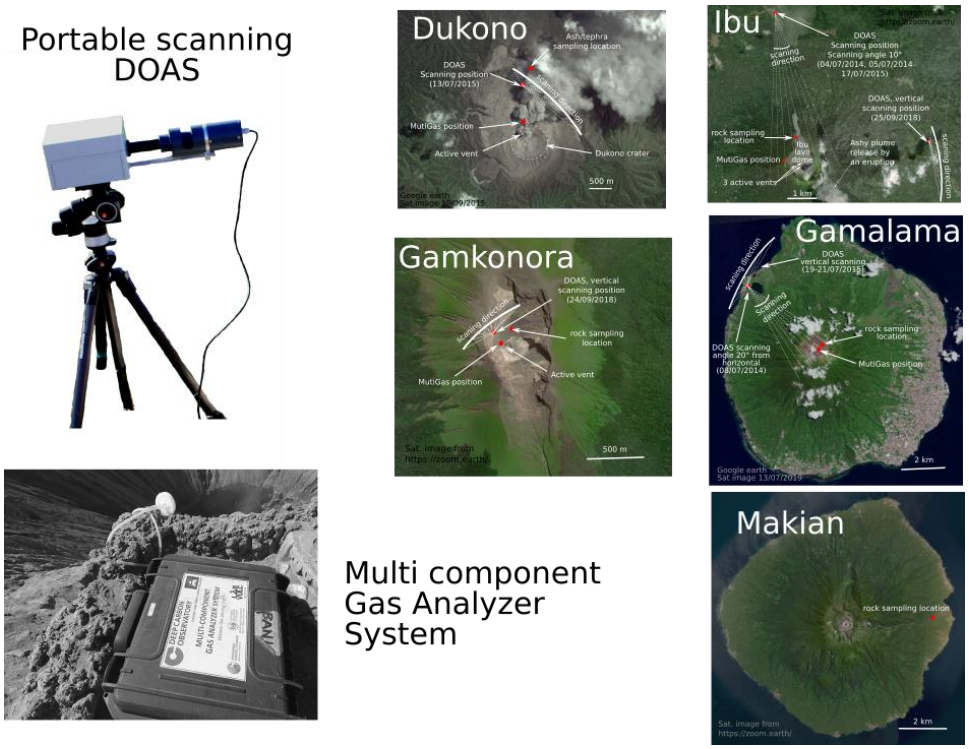

Figure 2. The pictures show the portable DOAS scanning and the MultiGAS systems used in this work. During measurements, the MultiGAS was positioned at the rim while the DOAS performed either vertical scanning or with a defined angle downwind. The positions of the instruments are indicated on each volcano. The rock sampling locations are also provided. On Makian, only rock samples were collected.

3-4-2. Ibu

To further constrain degassing of Ibu, new gas measurements were carried out at the rim of the crater using the MuitiGAS equipment and at a 5-6 km distance from the summit using the UV spectrometer scanning system. Scans were made in the vertical plane between elevations of 10° from horizontal depending on the wind direction (Fig.2). The eastern part of the crater rim is innaccessible and the MultiGAS recording was not continuously in the plume. When larger eruptions occurred, some of the emitted gas reached the gas sensors. We collected new samples from the viscous lava flow that extends beyond the crater.

3-4-3. Gamkonora

Rock sample locations are reported in Figure 2.

3-4-4. Gamalama

Fresh rock samples were collected at the summit and were likely recently ejected.

3-4-5. Makian

During our visit to the summit in 2014, there was no degassing and, consequently, no gas measurements were performed. Rock samples were collected in the depression that extends from the summit to the coast on the western part of the island (Fig.2).

5. Results

5-1. Arc degassing budget

Table 1 reports our SO_2 flux estimates for Ibu volcano based on UV DOAS. Our new SO_2 flux results for Ibu range between 50 and 140 Mg/d with a daily mean value of 105 Mg. This is an order of magnitude higher than the estimate reported by Saing et al. (2014) that corresponded to SO_2 released by explosions only. Our new estimate integrates both passive and eruptive discharges, and as such may be considered more representative of Ibu's bulk plume flux of SO_2 to the atmosphere.

Table 1. SO_2 flux estimates for Ibu and Gamalama volcanoes

Ibu volcano								Gamalama volcano	
04/07/2014		05/07/2014		17/07/2015		25/09/2018		08/07/2014	
Start time	SO_2 flux	Start time	SO_2 flux	Start time	SO_2 flux	Start time	SO_2 flux	Start time	SO_2 flux

(LT)	(kg/s)	(LT)	(kg/s)	(LT)	(kg/s)	(LT)	(kg/s)	(LT)	(kg/s)
10:27	1.6 ± 0.4	09:30	2.1 ± 0.5	10:44	0.6 ± 0.3	11:07	2.3 ± 0.7	11:21	0.4 ± 0.20
10:43	1.5 ± 0.4	09:44	1.6 ± 0.3	10:50	0.5 ± 0.4	11:10	0.9 ± 0.5	11:29	0.3 ± 0.13
10:50	1.6 ± 0.6	09:49	1.8 ± 0.3	10:56	1.0 ± 0.3	11:13	0.9 ± 0.5	11:35	0.1 ± 0.06
10:57	1.6 ± 0.6	09:53	1.7 ± 0.5	11:02	0.7 ± 0.4	11:16	0.9 ± 0.5	11:42	0.5 ± 0.23
11:03	1.7 ± 0.6	10:09	1.9 ± 0.5	11:08	0.6 ± 0.4	11:18	1.0 ± 0.6	11:50	0.5 ± 0.20
11:20	1.4 ± 0.6	10:16	1.3 ± 0.5	11:14	0.5 ± 0.4	**Mean value**	**1.2 ± 0.6**	11:59	0.1 ± 0.05
11:26	1.6 ± 0.6	10:24	1.1 ± 0.5	11:20	0.5 ± 0.4			12:05	0.1 ± 0.03
11:33	1.3 ± 0.6	10:30	1.0 ± 0.3	11:26	0.5 ± 0.3			12:13	0.1 ± 0.07
11:39	2.0 ± 0.6	10:35	0.6 ± 0.3	11:31	0.5 ± 0.4			12:20	0.3 ± 0.12
11:45	1.8 ± 0.6	**Mean value**	**1.4 ± 0.4**	11:37	0.5 ± 0.3			12:28	0.2 ± 0.08
Mean value	**1.6 ± 0.6**			11:42	0.7 ± 0.4			12:34	0.1 ± 0.03
				11:48	0.6 ± 0.4			12:40	0.1 ± 0.05
				11:53	0.5 ± 0.2			12:46	0.1 ± 0.03
				11:59	0.6 ± 0.4			12:53	0.1 ± 0.07
				12:58	0.8 ± 0.4				
				13:04	1.2 ± 0.4				
				13:09	0.6 ± 0.2				
				Mean value	**0.6 ± 0.3**				
On Ibu SO_2 emission rate fluctuated between 50 and 140 t/d with a mean value of 105 ± 40 t/d								**Mean SO_2 flux from Gamalama: 17 ± 9 t/d**	

Table 2 presents the first gas composition data for Ibu volcano and Figure 3 highlights the linear correlations between SO_2 and the other gases (H_2O, CO_2, H_2S, and H_2), confirming their common origin. The H_2O, CO_2, SO_2, H_2S, and H_2 abundances in the Ibu plume range between 500-2500, 370-380, 0.01-0.7, 0.3-0.9, and 1.2-3.0 ppmv, respectively. The gas-to-SO_2 ratios (obtained from the gradients of the best-fit regression lines in the scatter plots of Figure 3) are 93584, 13.4, 0.7, and 1.9 for H_2O/SO_2, CO_2/SO_2, H_2S/SO_2, and H_2/SO_2 respectively. Combing these ratios with the above mean SO_2 flux, indicates daily outputs of 67200 Mg of H_2O, 967 Mg of CO_2, 42 Mg of H_2S, and 6 Mg of H_2.

Table 2. Ibu gas composition and total emission budget.

Concentration range		
H_2O (ppm v)	500 - 2500	
CO_2 (ppm v)	370 - 385	
SO_2 (ppm v)	0.01 - 0.7	
H_2S (ppm v)	0.3 - 0.9	
H_2 (ppm v)	1.3 - 3.0	
Gas ratio		
H_2O/SO_2	2276 ± 1321	
CO_2/SO_2	13.4 ± 8.2	
H_2S/SO_2	0.7 ± 0.1	
H_2/SO_2	1.9 ± 0.9	
Composition (mol. %)		**Flux (t/d)**
H_2O	99.3 ± 0.1	67200 ± 14800
CO_2	0.6 ± 0.2	967 ± 280
SO_2	0.04 ± 0.02	105 ± 40
H_2S	0.03 ± 0.002	42 ± 6
H_2	0.08 ± 0.02	6 ± 2

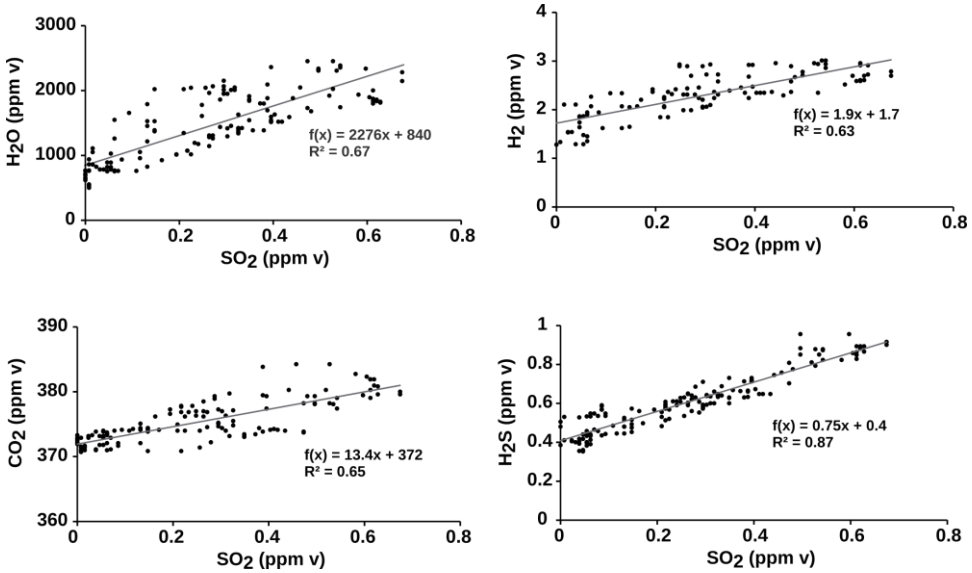

Figure 3. Gas to SO_2 linear correlations obtained on Ibu volcano using the MultiGAS sensor.

In contrast, during the DOAS measurements in July 2014, Gamalama exhibited passive degassing activity and hence the corresponding SO_2 flux result of 17 t (Table 1) may be considered as more representative of the volcanic system. When combining this mean SO_2 flux with the gas to SO_2 ratios obtained by Kunrat et al. (2020), the total gas emission budget for Gamalama corresponds to 15151 t, 888 t, 23 t, and 0.6 t of H_2O, CO_2, H_2S, and H_2 respectively.

Combining these new gas results for Ibu and Gamalama with the recent degassing estimates from Dukono and Gamkonora (Bani et al., 2017; Saing et al., 2020), one can estimate the total volcanic degassing budget from the Halmahera arc, considering the contribution from Makian negligible. Hence the total daily degassing budget for the Halmahera arc may correspond to 96300 t, 2093 t, 944 t, 79 t, and 15 t of H_2O, CO_2, SO_2, H_2S, and H_2 respectively (Table 3). Most of SO_2 and H_2 are released from Dukono, while Ibu releases the highest quantity of H_2O and H_2S, and finally both Gamalama and Ibu are releasing high CO_2 gas.

Table 3. Total degassing budget from Halmahera active volcanoes

	Dukono (Bani et al., 2018)		**Ibu (this work)**		**Gamkonora (Saing et al., 2020)**		**Gamalama (Kunrat et al., 2020; this work)**		**Arc emission budget**
	Gas comp.(mol. %)	**Gas flux (t/d)**	**Gas comp.(mol. %)**	**Gas flux (t/d)**	**Gas comp.(mol. %)**	**Gas flux (t/d)**	**Gas comp.(mol. %)**	**Gas flux (t/d)**	**(t/d)**
H_2O	97.2 ± 2.7	14000 ± 4000	99.3 ± 0.1	67200 ± 14800	94.7 ± 4.4	129 ± 53	97.5 ± 2.2	15000 ± 3000	96329 ± 27000
CO_2	0.6 ± 0.04	225 ± 69	0.6 ± 0.2	967 ± 280	3.9 ± 0.4	13 ± 5	2.3 ± 0.2	888 ± 74	2093 ± 450
SO_2	1.6 ± 0.4	819 ± 235	0.04 ± 0.02	105 ± 40	0.7 ± 0.3	3.4 ± 1.4	0.03 ± 0.02	17 ± 9	944 ± 400
H_2S	0.05 ± 0.01	13 ± 4	0.03 ± 0.002	42 ± 6	0.4 ± 0.01	1.1 ± 0.4	0.08 ± 0.005	22.6 ± 1.4	79 ± 20
H_2	0.48 ± 0.04	8 ± 2	0.08 ± 0.02	6 ± 2	0.2 ± 0.03	0.03 ± 0.01	0.04 ± 0.02	0.6 ± 0.3	15 ± 4
Mean CO_2/S_T	0.4 ± 0.1		8.4 ± 0.2		3.5 ± 0.7		20.9 ± 2.0		

Mean T (°C)*	691 ± 48	507 ± 37	670 ± 10	452 ± 39

** Gas equilibrium temperature calculated following Moussallam et al. (2018)*

The

5-2. Composition of the eruptive products

5-2-1. Major and trace elements

The major, trace, and isotope compositions of the fresh eruptive products sampled in this work are reported in Table 4. They display a wide range of silica content (SiO_2), varying from 50 wt% on Makian to more than 67 wt% on Ibu. Dukono, Gamkonora, and Gamalama exhibit intermediate SiO_2 contents of 56-58 wt%. If the TAS diagram (Fig.4), Makian rocks span the fields of basalt to basaltic andesites, whilst Ibu rocks are intermediate between dacites and trachytes (Saing et al. 2014). Dukono rocks plot in the domain of andesites to trachy-andesites (c.f. Bani et al. 2017). Gamkonora rocks also fall in the andesite domain but are lower in alkalis than Dukono. Older Gamkonora rocks (Badan Geologi, 2011) are slightly less evolved, and plot in the basaltic andesite field. Gamalama samples lie in the basaltic-andesite domain, comparable with products of 1907 and 1990 erupotions (Badan Geologi, 2011).

Table 4. Isotope ratios, major and trace element composition of the rock samples

	Dukono			**Ibu**			**Gamkonora**		**Gamalama**	**Makian**			
	DK1	**Dk2**	**DK3**	**IB-1**	**IB-2**	**IB-3**	**GK1**	**GK2**	**GL**	**MK1**	**MK2**	**MK3**	**MK4**
SiO_2 (wt%)	58.0	59.5	59.3	67.1	67.1	66.6	57.0	57.7	56.6	50.0	53.3	55.8	50.0
TiO_2	0.8	0.8	0.7	0.69	0.70	0.69	0.84	0.78	0.84	0.85	0.73	0.69	0.86
Al_2O_3	13.9	15.3	15.8	15.1	14.9	14.9	17.4	17.7	17.3	19.7	19.4	19.0	19.5
Fe_2O_3	10.5	8.4	8.6	5.0	5.0	5.0	9.0	8.8	9.5	9.2	8.7	7.7	9.2
MnO	0.2	0.2	0.1	0.146	0.146	0.147	0.180	0.177	0.182	0.164	0.165	0.158	0.162
MgO	2.0	2.7	2.3	0.84	0.85	0.85	3.08	3.20	3.49	6.04	4.49	3.35	5.72
CaO	7.3	5.8	6.0	3.00	2.97	3.00	6.84	6.95	7.26	10.64	8.47	7.54	10.44

Na_2O	3.1	3.4	3.5	4.42	4.38	4.35	3.78	3.74	3.45	3.20	3.67	3.92	3.20
K_2O	3.7	2.5	2.5	3.22	3.20	3.19	1.64	1.50	1.56	0.83	1.04	1.21	0.85
P_2O_5	0.4	0.3	0.3	0.186	0.185	0.188	0.304	0.255	0.192	0.149	0.157	0.159	0.153
LOI	-	-	-	-0.07	-0.07	0.05	-0.18	-0.34	-0.330	-0.180	-0.36	0.44	-0.280
Total	100.1	98.9	99.1	99.61	99.42	99.00	99.93	100.57	99.98	100.62	99.93	99.93	99.69
Rb (ppm)	25.2	24.4	9.7	75	74	74	37	26	39	20	24	29	19
Sr	476.3	469.3	354.1	270	268	267	407	415	346	404	308	335	413
Ba	213.9	214.1	116.3	522	549	516	442	284	317	205	205	237	214
Sc	-	-	-	15.9	16.6	16.0	22.8	21.5	26.5	37.7	25.8	20.7	36.2
V	269.2	259.3	361.7	16.2	16.9	16.4	193	211	227	288	217	189	279
Cr	41.5	49.9	<8.7	0.9	1.2	1.4	2.7	3.0	4.9	59.4	17.2	4.6	53.3
Co	21.3	21.0	29.8	4.6	4.4	4.5	22.5	22.0	25.4	30.7	25.0	20.3	30.4
Ni	14.8	14.1	12.2	1.6	1.3	2.0	5.4	7.0	7.1	32.2	19.3	9.7	31.1
Y	15.7	15.0	21.5	38.4	38.7	38.7	32.8	28.2	28.4	23.1	24.2	24.7	23.6
Zr	60.5	59.9	51.0	178	178	176	122	98.7	119	74.2	101	107	72.9
Nb	0.9	0.9	0.6	3.6	3.7	3.5	3.5	2.8	2.9	2.0	2.5	2.6	1.0
La	6.7	6.7	8.0	15.1	14.7	14.7	13.2	9.5	17.8	11.0	10.3	10.0	11.4
Ce	15.0	14.6	19.5	31.9	31.4	33.6	30.1	24.3	38.1	23.8	24.1	24.5	26.3
Nd	9.6	9.4	12.1	21.4	21.7	21.0	19.4	15.6	21.0	14.4	13.0	12.0	15.0
Sm	2.3	2.5	2.8	5.2	5.6	5.5	4.5	4.0	4.4	3.6	2.7	2.3	2.7
Eu	0.8	0.7	1.0	1.38	1.36	1.49	1.47	1.19	1.39	1.11	0.94	0.94	0.98
Gd	2.9	2.6	3.0	6.2	5.9	6.0	4.9	4.0	4.8	3.4	3.4	3.0	3.7
Dy	-	-	-	6.1	6.2	6.1	5.2	4.5	4.6	3.1	3.3	3.1	3.2
Er	-	-	-	3.7	3.9	3.9	3.1	2.7	2.6	1.9	2.2	1.9	1.7
Yb	1.6	1.7	2.5	4.14	4.09	4.10	3.31	2.98	2.91	1.90	2.11	2.06	1.86
Lu	0.3	0.3	0.4	-	-	-	-	-	-	-	-	-	-
Th	1.0	1.0	0.5	3.8	3.7	3.5	3.6	1.8	6.5	3.1	3.2	3.2	3.1
$^{87}Sr/^{86}Sr$	0.70386			0.70394	0.70395	0.70394	0.70398	0.70411	0.70411		0.70438	0.70424	
$^{143}Nd/^{144}Nd$	0.51299			-	-	0.512981	0.51295	0.51294	0.512835		0.51284	0.51286	
$^{206}Pb/^{204}Pb$	18.51460			18.5862	18.5891	18.5610	18.5766	18.6277	18.6100		18.5668	18.5573	
$^{207}Pb/^{204}Pb$	15.5960			15.6175	15.6206	15.5814	15.5932	15.6344	15.6104		15.5956	15.5917	
$^{208}Pb/^{204}Pb$	38.4778			38.6124	38.6209	38.5087	38.5500	38.6885	38.6465		38.5668	38.5364	

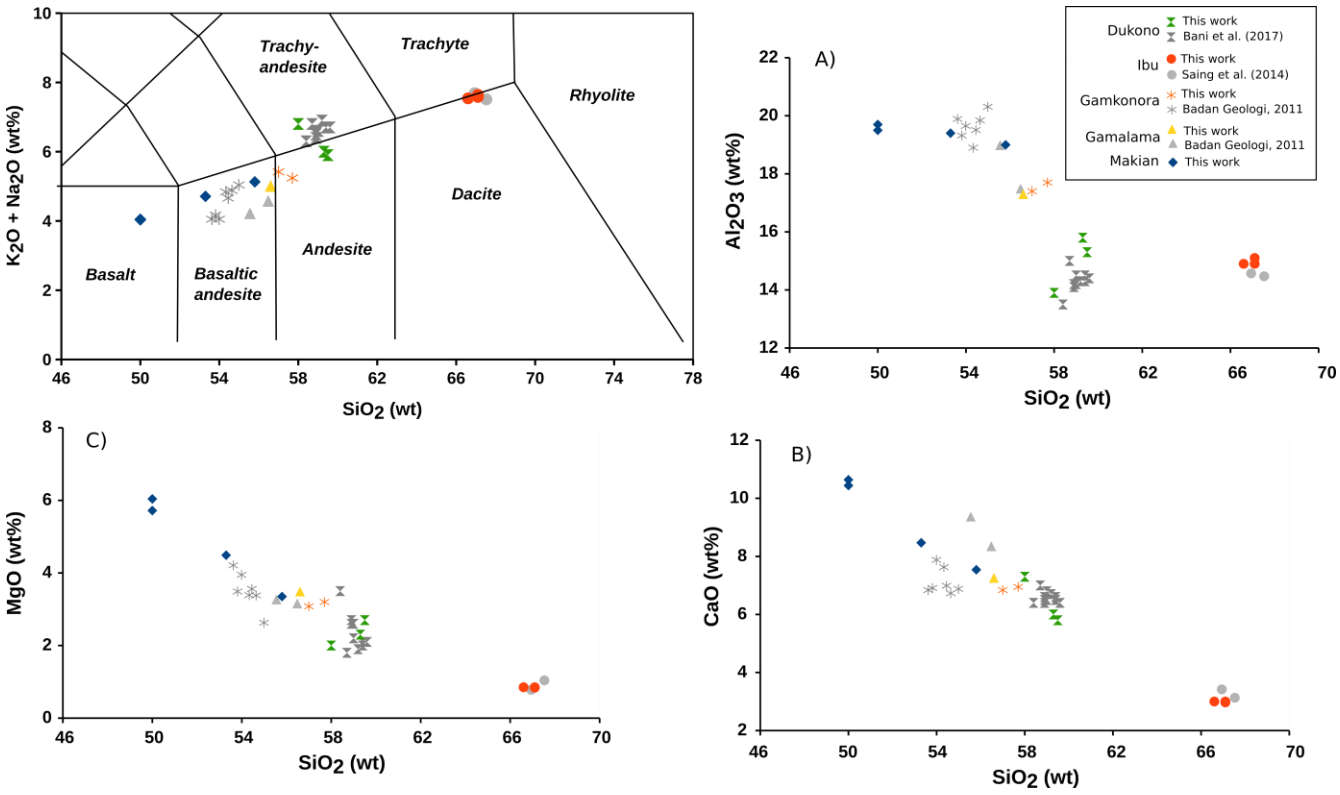

Figure 4. Major element oxides for Halmehara active volcanoes range from basalt to dacite and trachyte. The most differentiated rocks occur on Ibu whilst the least are from Makian. Dukono samples are relatively higher in alkalis. Al_2O_3, CaO, and MgO correlations with SiO_2 show a negative trend from Makian to Ibu. Data from the literature shown in grey.

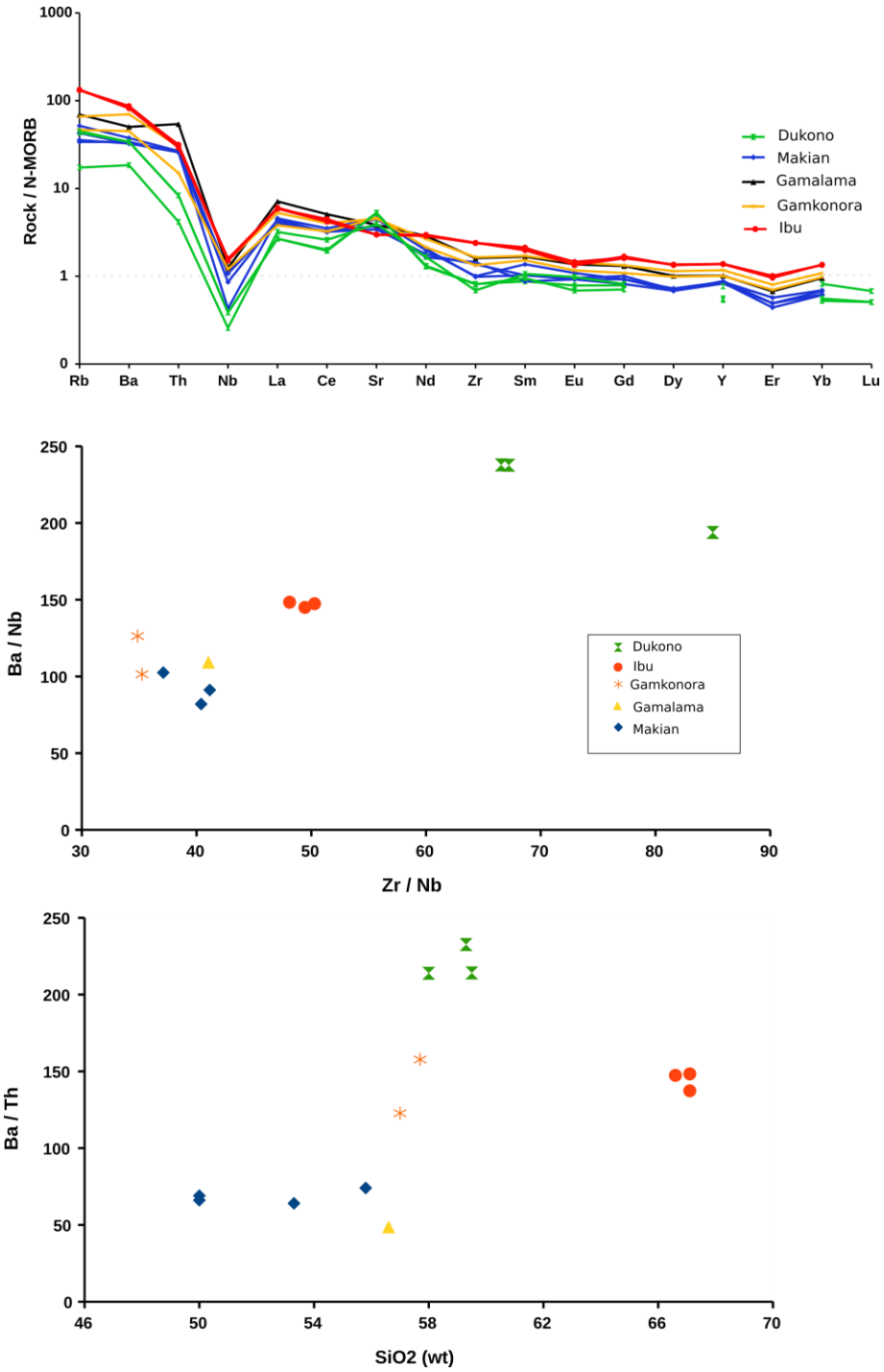

Figure 5. Trace element concentrations normalized to N-MORB (Hofmann, 1988) indicate typical arc magmas. Ba/Nb vs. Zr/Nb and Ba/Th vs. SiO_2 (wt%) vary between Halmahera volcanoes and highlight Dukono as sustained by a fluid dominated regime.

The MgO, CaO, and Al_2O_3 vs. SiO_2 (wt%) scatter plots (Fig.4) define a negative correlation array

stretching from Makian in the south, where the most mafic compositions are observed, to Ibu in the north of the Halmahera arc (where magmas are more evolved). Dukono displays the lowest Al_2O_3 contents whilst Ibu exhibits the lowest MgO and CaO contents. Makian samples in contrast display the highest Al_2O_3, CaO, and MgO contents. Again the older rocks from Gamkonora are more enriched in Al_2O_3 compared with the current magmas. Overall, the rock compositions of the recent volcanic products obtained in this work (Table 4) range from more mafic to the south of the arc to more evolved in the northern part of the arc. One particularity evidenced by these major elements is the enriched alkali contents in the samples from Dukono, relative to the other volcanoes of the arc (Fig.4). This is possibly due to the farthest distance of Dukono volcano from the subduction trench in comparison to other volcanoes.

Trace-element concentrations (Table 4) exhibit the typical signatures of arc magmas, with enrichments in highly incompatible elements (e.g., Ba contents range from 200 to 550 ppm), and negative Nb anomalies (Fig.5). The flat MREE to HREE (Sm/Yb between 1,13 to 1,89) patterns suggest lack of residual garnet in the mantle source. All trace element patterns are identical, except the low Sr contents on Ibu that contrast with the positive Sr anomaly of the other samples. In terms of trace element ratios, Ba/Th, Ba/Nb, and Zr/Nb vary respectively from 49 (Gamalama) to 233 (Dukono), from 82 (Gamalama) to 238 (Dukono), and from 35 (Gamkonora) to 85 (Dukono). In the Ba/Nb vs. Zr/Nb diagram (Fig.5), we observe a positive correlation where the Dukono samples display higher Ba/Nb at a given Zr/Nb ratio compared to Makian samples. We note that, except for the Gamalama sample, the Ba/Th ratios increase with increasing SiO_2 content (Fig.5). Lavas from Dukono have the highest Ba/Th ratios (214-237). Elevated Th/La ratios are typical for arc volcanic products (Plank, 2005), but again here Dukono displays low Th/La ratios of <0.15 compared to 0.19-0.37 for the other Halmehara volcano. Makian and Gamalama show the highest Th/La ratios (0.27-0.37).

5-2-2. Sr, Nd and Pb isotope variability

The Pb isotopic ratios range from 18.482 to 18.628 for $^{206}Pb/^{204}Pb$, from 15.554 to 15.634 for $^{207}Pb/^{204}Pb$ and from 38.356 to 38.689 for $^{208}Pb/^{204}Pb$. These results lie within the accepted range for the Halmahera arc in a $^{207}Pb/^{204}Pb$ vs $^{206}Pb/^{204}Pb$ diagram (Fig.6; Elburg and Foden, 1998). The Pb isotopes identify positive correlations in both $^{207}Pb/^{204}Pb$ vs. $^{206}Pb/^{204}Pb$ and $^{208}Pb/^{204}Pb$ vs. $^{206}Pb/^{204}Pb$ spaces, with Dukono and Gamalama plotting as end-members. Dukono exhibits the least radiogenic Pb signature.

Our new results identify a negative correlation in a $^{143}Nd/^{144}Nd$ vs. $^{87}Sr/^{86}Sr$ diagram (Fig.6), with $^{87}Sr/^{86}Sr$ values ranging between 0.70386 (Dukono) and 0.70438 (Makian) and $^{143}Nd/^{144}Nd$ values between 0.512846 (Makian) to 0.512995 (Dukono). Again, Dukono displays the highest $^{143}Nd/^{144}Nd$ ratio whilst Gamalama and Makian have the lowest $^{143}Nd/^{144}Nd$ ratio. The $^{143}Nd/^{144}Nd$ ratio from Ibu samples is higher than for Gamkonora rocks but is relatively lower than for Dukono samples. Makian samples have the most radiogenic $^{87}Sr/^{86}Sr$ ratios and a negative correlation is in the $^{87}Sr/^{86}Sr$ vs. Ba/Th diagram, from Makian-Gamalama to Dukono.

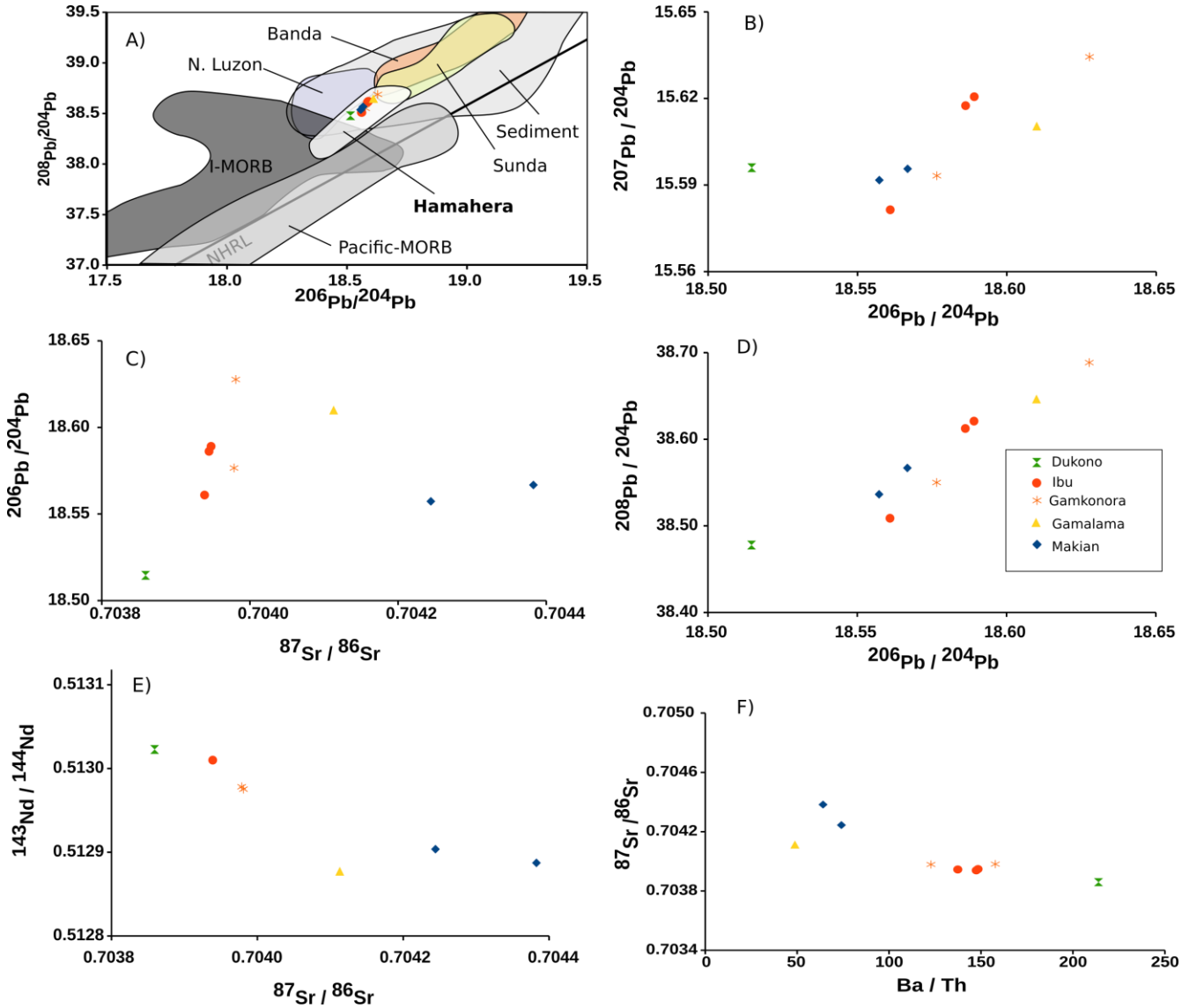

Figure 6. Pb isotopic ratios fall in the defined field of Halmahera arc (Elburg and Foden, 1998)(A). 207Pb/204Pb vs. 206Pb/204Pb and 208Pb/204Pb vs. 206Pb/204Pb show are positive correlation from Dukono to Gamalama (B, D). Makian samples have high 87Sr/86Sr ratios compare to other volcanoes (C). 143Nd/144Nd vs. 87Sr/86Sr diagram shows a negative correlation from Dukono to Makian (E). 87Sr/86Sr vs. Ba/Th also a negative correlation from Makian-Gamalama to Dukono.

6. Discussion

6-1. Arc-scale degassing budget

The volcanic emission budget from the Indonesia arcs has so far been estimated based on inferences and extrapolations (Andres and Kagnoc, 1998; Halmer et al., 2002; Aiuppa et al., 2019; Fischer et al., 2019; Bani et al., 2020), since direct measurements are available for only a few volcanoes. The most exhaustive volcanic degassing inventory for the archipelago is that of Carn et al. (2017) based on satellite observations. However, it represents only 20 out of 78 volcanoes in Indonesia (Siebert et al., 2010). Dukono is the only representative for the Halmahera arc, but with an emission rate double the ground-based estimate of 819 Mg/d (Table 3). According to Bani et al (2017), this high estimate from satellite data may due to over-sampling of more vigorous explosive periods.

Our ground-based observations indicate a total annual SO_2 output from all the Halmahera volcanoes of 0.34 ± 0.15 Tg. Dukono is the main SO_2 degassing source, representing 83% of the total SO_2 release from the arc. The Halmahera arc-scale SO_2 degassing exceeds the annual SO_2 release from the volcanoes of New Zealand (0.15 Tg/yr) or the Philippines (0.27 Tg/yr) (Fischer et al., 2019). It represents ~13% of the total SO_2 release from the Indonesian archipelago (2.56 Tg/yr) and ~4% of the global volcanic SO_2 degassing budget (8.80 Tg/yr) (Fischer et al., 2019).

Our estimate of the CO_2 emission budget for the Halmahera arc amounts to 0.76±0.16 Tg/yr. This represents ~10% of the Indonesian volcanic CO_2 degassing budget and ~1.4% of the global volcanic CO_2 budget. We caution, however, that roughly half of the Halmahera arc CO_2 budget is contributed by Ibu (Tab. 3), whose CO_2/SO_2 ratio signature (and, hence, the CO_2 flux) is inferred from brief measurements of a dilute (< 1 ppm SO_2) plume (see below). We estimate annual emissions of ~0.03 Tg of H_2S and ~0.005 Tg of H_2 from the Halmahera arc.

6-2. Variation in volcanic CO_2/S_T ratios

The volcanic gas CO_2/S_T ratio is widely used to investigate the genesis of volcanic arc volatiles (e.g., Saal et a., 2002; Aiuppa et al., 2014, 2017, 2019; Freundt et al., 2014). In interpreting the

variability of CO_2/S_T ratios observed in for the Halmahera volcanoes (Table 3) we must consider (i) the overprinting of magmatic signatures by shallow hydrothermal processes (scrubbing or reactive S; mixing and dilution with meteoric fluids) and (ii) the temporal paucity of data (e.g., Aiuppa et al. (2017), At Gamalama, Kunrat et al. (2020) point to extensive hydrothermal S scrubbing (Symonds et al., 2001), which is corroborated by the CO_2-SO_2-H_2S diagram (Fig.7; Stix and de Moor, 2018), in which Gamalala plots in the "S loss, scrubbing" field. This implies that the Gamalala high CO_2/S_T ratio of 20.9 is more a signature of shallow hydrothermal reactions than of the magmatic source. Hydrothermal processing is also likely at Gamkonora and Ibu, in view of the relatively high abundances of H_2S, with H_2S/SO_2 ratios of ~0.57 and 0.75, respectively (see also Fig. 7a). These also suggest hydrothermal influence on the measured gas CO_2/S_T ratios (of respectively 3.5 and 8.4).

The data for Ibu plot in the "deep hydrothermal-magmatic" field of Stix and de Moor, 2018; Fig. 7a. However, this classification is problematic because the measurements represent a snapshot in time and were made right after an explosion. It is thus very likely that the high CO_2/S_T ratio measured (8.4) reflects transient emission of deeply originated (CO_2-rich) gas during the explosive gas burst, as seen elsewhere (Oppenheimer et al., 2001; Burton et al., 2007). Aiuppa et al. (2017) already noted that gas emissions from lava domes are systematically S-poor (and/or C-rich) compared with emissions associated with mafic volcanism at equivalent temperature, interpreted as a sign of pervasive circulation of meteoric fluids in domes (and consequent S-scrubbing). The high CO_2/S_T ratio observed at Ibu may similarly reflect gas-water-rock interactions occurring within the dome.

Only the CO_2-SO_2-H_2S data for Dukono (Fig 7a), are likely representative of shallow magma degassing with negligible hydrothermal influence. Its very low CO_2/S_T ratio of 0.4 (Bani et al., 2018) corresponds with the CO_2/S_T ratio of a depleted mantle source (0.3 to 0.8 Saal et al, 2002; Aiuppa et al., 2017; 2019). In combination with its whole-rock Ba/La ratio (Fig.7; a trace-element proxy for slab-derived fluids; Hawkesworth et al., 1993), the Dukono gas CO_2/S_T of 0.4 suggests limited C supply from

subducted sediments (Aiuppa et al., 2017). The relatively distant location of Dukono (>80 km) from the Halmahera trench may play a role in this minor subducted sediment contribution.

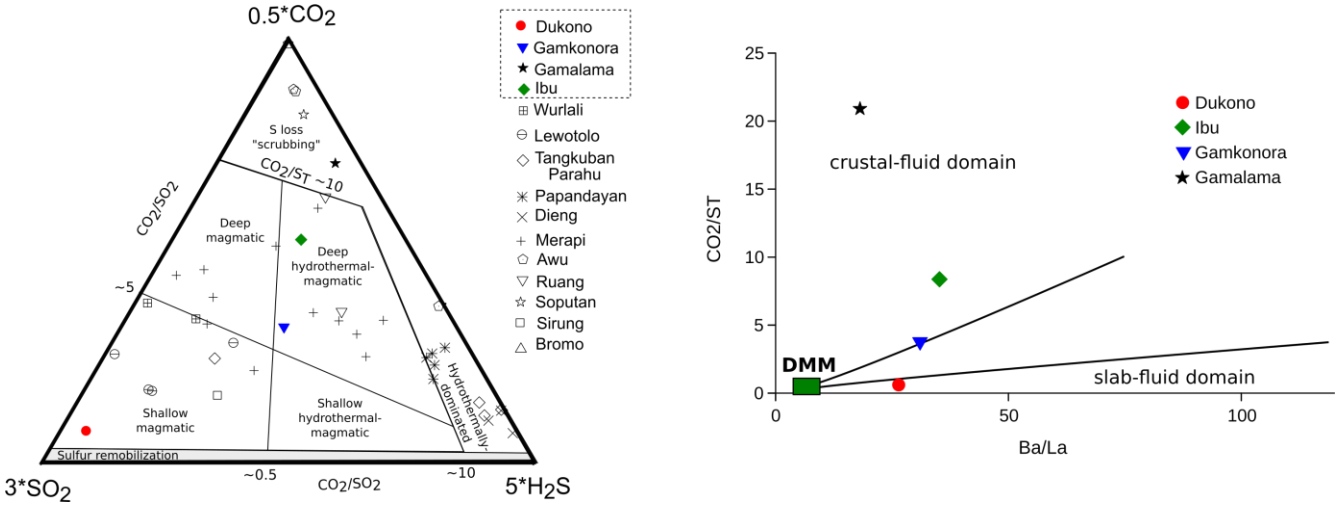

Figure 7. The CO_2-SO_2-H_2S diagram shows the strong influence of hydrothermal on Gamalama's emissions. The gas compositions from other Indonesian volcanoes are presented for comparison (modified from Bani et al., 2020). The CO_2/ST vs Ba/La figure indicates slab-volatile contribution at Dukono whereas Gamkonora, Ibu, and possibly Gamalama receive volatiles from subducted sediments. (DMM = Depleted MORB Mantle).

6-3. Fluid fluxing and sediment recycling

Our isotopic measurements (Table 4) lie within the Halmahera arc compositional domain (Fig.6). However, we note increases in $^{206}Pb/^{204}Pb$, $^{207}Pb/^{204}Pb$, and $^{208}Pb/^{204}/Pb$ ratios from Dukono to the other volcanoes of Halmahera. High Pb isotopic ratios suggest incorporation of subducted sediments in the source magmas. This would suggest limited contribution of subducted sediment to Dukono magmas, consistent with the very low CO_2/S_T ratio that we measured. There is perhaps a weak trend of increasing Pb isotopic ratios from Makian to Ibu, Gamkonora, and Gamalama. More convincingly, the Nd and Sr isotopic ratios discriminate the effects of sediment recycling in the magma sources along the Halmahera arc (Fig.6). Increasing sediment contributions in the mantle source impart

low $^{143}Nd/^{144}Nd$ ratios and high $^{87}Sr/^{86}Sr$ ratio to magmas (e.g., Ben Othman et al., 1989). On this basis, there is a clear decrease in recycled sediment contribution from the south to the north in the Halmahera arc (Fig.8). Makian has the strongest sediment signature in its magma, followed to the north by Gamalama, Gamkonora, Ibu, and finally Dukono with the least sediment recycling component (Fig.8).

Dukono samples have the most radiogenic $^{143}Nd/^{144}Nd$ ratio but the least radiogenic $^{87}Sr/^{86}Sr$ and $^{206}Pb/^{204}Pb$ ratios (Fig.6) suggesting a dominant mantle contribution to the source magma. But Halmahera volcanoes tap a depleted mantle source (Macpherson et al., 2003; Bani et al., 2018) implying high fluid fluxes to lower the solidus and promote melting. This is the case for Dukono, as highlighted by very high Zr/Nb ratios (Fig.5). Indeed, a mantle that has previously lost a basaltic melt fraction is depleted in highly incompatible elements (Macpherson et al., 2003). Any incoming fluid will impart a broad correlation between Zr/Nb and Ba/Nd (Keppler, 1996; Macpherson et al., 2003; Bani et al., 2018) as seen in Figure 5. Dukono is thus subjected to a fluid dominant regime (Fig.8). At the arc scale, recognising that high fluid fluxes can induce high Ba/Th ratio and low Sr isotopic ratios (Alburg and Foden, 1998; Elburg et al., 2002), the Ba/Th vs. $^{87}Sr/^{86}Sr$ diagram (Fig.8) indicates a relative increase of fluid fluxes along the arc, from Makian to Dukono. It also implies that the fluid is generated as a result of dehydration of altered oceanic crust (Turner et al., 1997) that progressively dominates to the north of the arc, corresponding to decreasing slab-sediment contribution. As for the increase of fluid fluxes away from the trench, Macpherson et al. (2003) and Elliott et al.(1997) have argued that the steepening of the subducted slab, the downward force from the Philippine sea plate, and the westward motion of continental fragments along the Sorong fault, have enhanced mantle wedge compression leading to high fluid fluxes, as observed at Dukono (Bani et al., 2018).

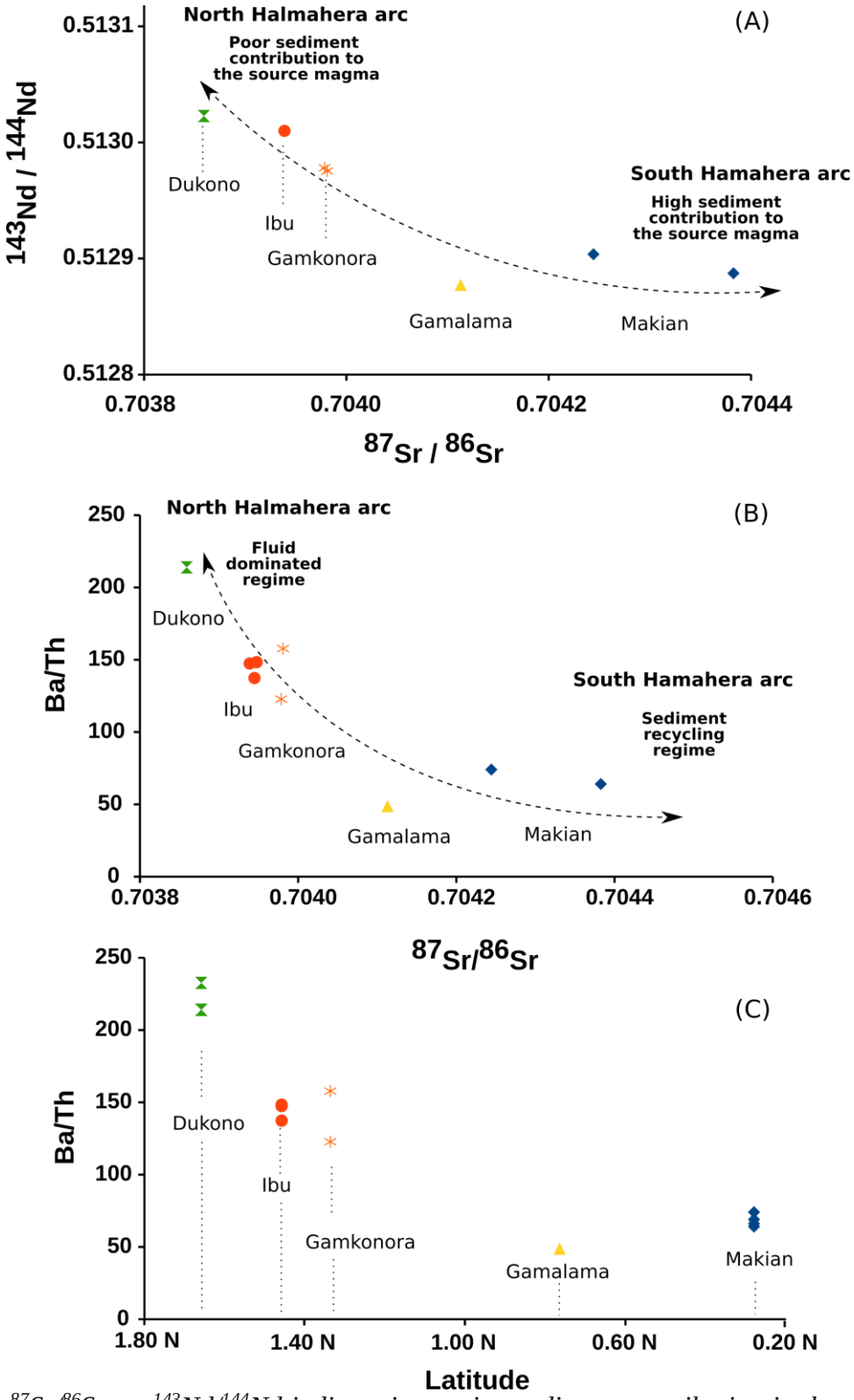

Figure 8. A) $^{87}Sr/^{86}Sr$ vs. $^{143}Nd/^{144}Nd$ indicate increasing sediment contribution in the source magma from north to south in the Halmahera arc. B) The Ba/Th vs. $^{87}Sr/^{86}Sr$ distribution indicates progressive

increase of fluid flux from south to north in the arc. C) The latitude of each volcano is plotted against Ba/Th emphasizing the isotope and trace element changes along the arc.

6-4. Comparison of recent ejecta with Halmahera Neogene and Quaternary sources

The evolution of the source magmas of the Halmahera arc throughout Neogene and Quaternary is described by Macpherson et al. (2003) and summarized in Figure 9. $^{206}Pb/^{204}Pb$, $^{207}Pb/^{204}Pb$, and $^{208}Pb/^{204}Pb$ ratios have increased from Neogene to Quaternary indicating increasing sediment contribution. Our Pb isotope results are comparable to the former values suggesting the source mechanism sustaining volcanic activity is the same as that of early Quaternary. However, while the $^{143}Nd/^{144}Nd$ ratios of Makian and Gamalama (south Halmahera arc) are comparable with the Quaternary source, those for Gamkonora, Ibu, and Dukono (north Halmahera arc) are similar to the Neogene source. The change of $^{143}Nd/^{144}Nd$ ratios observed between Neogene and Quaternary is potentially comparable currently situation along the arc with more sediment signatures in the magma sources of the southern volcanoes (Makian, Gamalama) compare to Dukono, Ibu, and Gamkonora in the North (Fig.9).

In contrast, instead of increasing from Neogene to Quarternary (Fig.9) as might be expected with increasing sediment in the source, the Ba/Nd and Zr/Nd ratios show a clear decrease from Neogene to Quaternary. This led Macpherson et al. (2003) to argue that the Neogene to Quaternary evolution was induced by a compositional change in the mantle wedge rather than from sediment incorporation. Our measurements reveal higher Ba/Nd and Zr/Nd ratios compared with the Quaternary source but are coherent with the rest of our findings, emphasizing the role of sediment recycling. Had there been a change of composition in the mantle wedge between Neogene and Quaternary then, based on the distinct Ba/Nd and Zr/Nd ratios we record, it appears that the mantle wedge composition has changed again.

340

Figure 9. a) Decreasing $^{143}Nd/^{144}Nd$ ratios from Quaternary to Neogene. Samples from Ibu, Dukono and Gamkonora fall in the Neogene group whilst Gamalama and Makian appear in the Quaternary

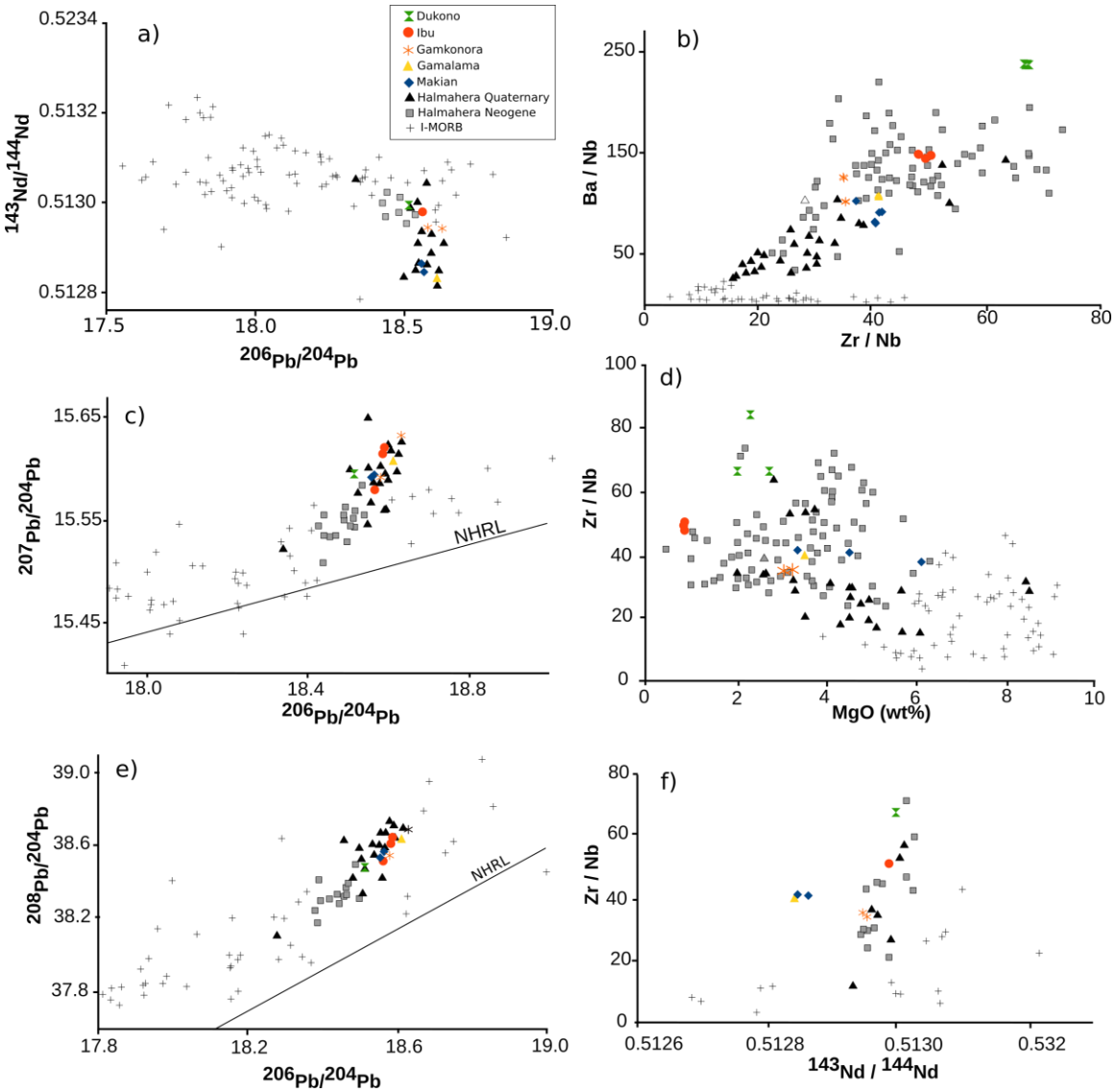

group. b) Quaternary source has a lower Ba/Nd and Zr/Nd compare to Neogene. All the recent sample plotted in the Neogene group. c;e) Increase in $^{206}Pb/^{204}Pb$, $^{207}Pb/^{204}Pb$ and $^{208}Pb/^{204}Pb$ ratios from

345 *Neogene to Quaternary. Recent product occur in the Quaternary group. d) Zr/Nb from Quaternary and Neogene are well above the I-MORB and a specific Zr/Nb range. Recent products also display a well*

defined Zr/Nb range except for Dukono which has higher Zr/Nb. f) Quaternary and Neogene products fall in defined $^{143}Nd/^{144}Nd$ ratios. The recent ejecta show an increase of $^{143}Nd/^{144}Nd$ from south to north in the Halmahere arc.

7. Conclusions

We have reported the first arc-scale gas emission budget for the Halmahera arc, indicating daily fluxes of the order of 96300 Mg of H_2O, 2093 Mg CO_2, 944 Mg SO_2, 79 Mg of H_2S and 15 Mg of H_2. The main SO_2 and H_2 source from the arc is Dukono, while Ibu releases the highest quantity of H_2O and H_2S. Gamalama and Ibu are the main sources of CO_2. CO_2/S_T ratios indicate a relationship with distance of the volcano from the trench. Dukono, situated about 80 km from the trench, is a CO_2-poor gas source compared with the other volcanoes of the arc, although hydrothermal processes complicate the picture for the other volcanoes. Geochemistry and isotope geochemistry of recent ejecta are consistent with the varying contribution of subducted sediment to volatile fluxes and emphasize the role of high fluid flux into the mantle wedge and partial melting of depleted mantle. Dukono represents a fluid dominant regime and the mantle contribution is preponderant in its source magma. Lead, neodymium and strontium isotopic data along with Ba/Nd, Zr/Nd, Ba/Th and Zr/Nb ratios also highlight compositional variability of magma sources along the Halmahera arc, indicating progressive decrease of sediment contribution from south (Makian, Gamalama) to north (Gamkonora, Ibu, Dukono). The fluid formed by dehydration of altered oceanic crust becomes more conspicuous for the northerly volcanoes. Isotopic trends between the Neogene and Quaternary are comparable to the current compositional variability of magma between the north and south of the Halmahera arc.

Acknowledgments

A.A. acknowledges funding from the DECEDE initiative of the Deep Carbon Observatory and from the MIUR (under grant PRIN2017-2017LMNLAW).

References

Agustan, Kimata, F., Abidin, H.Z., Pamitro, Y.E., 2010. Measuring ground deformation of the tropical volcano, Ibu, using ALOS-PALSAR data. Remote Sensing Letters 1, 37–44. https://doi.org/10.1080/01431160903246717

Aiuppa, A., Tamburello, G., Napoli, R.D., Cardellini, C., Chiodini, G., Giudice, G., Grassa, F., Pedone, M., 2013. First observations of the fumarolic gas output from a restless caldera: Implications for the current period of unrest (2005–2013) at Campi Flegrei. Geochemistry, Geophysics, Geosystems 14, 4153–4169. https://doi.org/10.1002/ggge.20261

Aiuppa, A., Robidoux, P., Tamburello, G., Conde, V., Galle, B., Avard, G., Bagnato, E., De Moor, J.M., Martínez, M., Muñóz, A., 2014. Gas measurements from the Costa Rica–Nicaragua volcanic segment suggest possible along-arc variations in volcanic gas chemistry. Earth and Planetary Science Letters 407, 134–147. https://doi.org/10.1016/j.epsl.2014.09.041

Aiuppa, A., Fischer, T.P., Plank, T., Robidoux, P., Di Napoli, R., 2017. Along-arc, inter-arc and arc-to-arc variations in volcanic gas CO_2/S_T ratios reveal dual source of carbon in arc volcanism. Earth-Science Reviews 168, 24–47. https://doi.org/10.1016/j.earscirev.2017.03.005

Aiuppa, A., Fischer, T.P., Plank, T., Bani, P., 2019. CO_2 flux emissions from the Earth's most actively degassing volcanoes, 2005–2015. Scientific Reports 9, 5442. https://doi.org/10.1038/s41598-019-41901-y

Andres, R.J., Kasgnoc, A.D., 1998. A time-averaged inventory of subaerial volcanic sulfur emissions. Journal of Geophysical Research: Atmospheres 103, 25251–25261. https://doi.org/10.1029/98JD02091

Badan-Geologi. Data Dasar Gunung Api, Wilaya Timur, 2nd ed.; Kementerian Energi dan Sumber DayaMineral: Jakarta, Indonesia, 2011; pp. 1–450.

Baker, S., Hall, R., Forde, E., 1994. Geology and jungle fieldwork in eastern Indonesia. Geology Today 10, 18–23. https://doi.org/10.1111/j.1365-2451.1994.tb00853.x

Bani, P., Oppenheimer, C., Allard, P., Shinohara, H., Tsanev, V., Carn, S., Lardy, M., Garaebiti, E., 2012. First estimate of volcanic SO_2 budget for Vanuatu island arc. Journal of Volcanology and Geothermal Research 211–212, 36–46. https://doi.org/10.1016/j.jvolgeores.2011.10.005

Bani, P., Tamburello, G., Rose-Koga, E.F., Liuzzo, M., Aiuppa, A., Cluzel, N., Amat, I., Syahbana, D.K., Gunawan, H., Bitetto, M., 2017. Dukono, the predominant source of volcanic degassing in Indonesia, sustained by a depleted Indian-MORB. Bull Volcanol 80, 5. https://doi.org/10.1007/s00445-017-1178-9

Bani, P., Le Glas, E., Kristianto, Aiuppa, A., Bitetto, M., Syahbana, D.K., 2020. Elevated CO_2 Emissions during Magmatic-Hydrothermal Degassing at Awu Volcano, Sangihe Arc, Indonesia. Geosciences 10, 470. https://doi.org/10.3390/geosciences10110470

Barrat, J.A., Keller, F., Amossé, J., Taylor, R.N., Nesbitt, R.W., Hirata, T., 1996. Determination of Rare Earth Elements in Sixteen Silicate Reference Samples by Icp-Ms After Tm Addition and Ion Exchange Separation. Geostandards Newsletter 20, 133–139. https://doi.org/10.1111/j.1751-908X.1996.tb00177.x

Bertrand, J. (Ed.), 2003. Conflict in Maluku, in: Nationalism and Ethnic Conflict in Indonesia, Cambridge Asia-Pacific Studies. Cambridge University Press, Cambridge, pp. 114–134. https://doi.org/10.1017/CBO9780511559341.009

Bogumil, K., Orphal, J., Homann, T., Voigt, S., Spietz, P., Fleischmann, O.C., Vogel, A., Hartmann, M., Kromminga, H., Bovensmann, H., Frerick, J., Burrows, J.P., 2003. Measurements of molecular absorption spectra with the SCIAMACHY pre-flight model: instrument characterization and

reference data for atmospheric remote-sensing in the 230–2380 nm region. Journal of Photochemistry and Photobiology A: Chemistry, Atmospheric Photochemistry 157, 167–184. https://doi.org/10.1016/S1010-6030(03)00062-5

Buck, A., 1981. New Equations for Computing Vapor Pressure and Enhancement Factor. Journal of Applied Meteorology (1962-1982), 20(12), 1527-1532.

Carn, S.A., Fioletov, V.E., McLinden, C.A., Li, C., Krotkov, N.A., 2017. A decade of global volcanic SO 2 emissions measured from space. Scientific Reports 7, 44095. https://doi.org/10.1038/srep44095

Elburg, M.A., van Bergen, M., Hoogewerff, J., Foden, J., Vroon, P., Zulkarnain, I., Nasution, A., 2002. Geochemical trends across an arc-continent collision zone: magma sources and slab-wedge transfer processes below the Pantar Strait volcanoes, Indonesia. Geochimica et Cosmochimica Acta 66, 2771–2789. https://doi.org/10.1016/S0016-7037(02)00868-2

Elliott, T., Plank, T., Zindler, A., White, W., Bourdon, B., 1997. Element transport from slab to volcanic front at the Mariana arc. Journal of Geophysical Research: Solid Earth 102, 14991–15019. https://doi.org/10.1029/97JB00788

Fischer, T.P., Arellano, S., Carn, S., Aiuppa, A., Galle, B., Allard, P., Lopez, T., Shinohara, H., Kelly, P., Werner, C., Cardellini, C., Chiodini, G., 2019. The emissions of CO_2 and other volatiles from the world's subaerial volcanoes. Scientific Reports 9, 18716. https://doi.org/10.1038/s41598-019-54682-1

Forde, E.J., 1997. The geochemistry of the Neogene Halmahera Arc, eastern Indonesia (Doctoral). Doctoral thesis, UCL (University College London). UCL (University College London).

Freundt, A., Grevemeyer, I., Rabbel, W., Hansteen, T.H., Hensen, C., Wehrmann, H., Kutterolf, S., Halama, R., Frische, M., 2014. Volatile (H2O, CO2, Cl, S) budget of the Central American

subduction zone. Int J Earth Sci (Geol Rundsch) 103, 2101–2127. https://doi.org/10.1007/s00531-014-1001-1

Galer, S.J.G., Abouchami, W., 1998. Practical application of lead triple spiking for correction of instrumental mass discrimination. Min. Mag.,62A, pp.491-492

Global Volcanism Program, 2013. Makian (268070), in, Volcanoes of the World, v. 4.9.1 (17 Sep 2020). Venzke, E (ed.). Smithsonian Institution. Downloaded 19 Nov 2020 (https://volcano.si.edu/volcano.cfm?vn=268070). https://doi.org/10.5479/si.GVP.VOTW4-2013

Global Volcanism Program, 2013. Dukono (268010), in, Volcanoes of the World, v. 4.9.1 (17 Sep 2020). Venzke, E (ed.). Smithsonian Institution. Downloaded 05 Dec 2020 (https://volcano.si.edu/volcano.cfm?vn=268010). https://doi.org/10.5479/si.GVP.VOTW4-2013

Global Volcanism Program, 2013. Gamalama (268060), in Volcanoes of the World, v. 4.9.1 (17 Sep 2020). Venzke, E (ed.). Smithsonian Institution. Downloaded 12 Dec 2020 (https://volcano.si.edu/volcano.cfm?vn=268060). https://doi.org/10.5479/si.GVP.VOTW4-2013

Goss, J., 2000. Understanding the Maluku Wars : Overview of Sources of Communal Conflict and Prospects for Peace. CAKALELE 11, 7–39.

Hall, R., 1987. Plate boundary evolution in the Halmahera region, Indonesia. Tectonophysics 144, 337–352. https://doi.org/10.1016/0040-1951(87)90301-5

Hall, R., Wilson, M.E.J., 2000. Neogene sutures in eastern Indonesia. Journal of Asian Earth Sciences 18, 781–808. https://doi.org/10.1016/S1367-9120(00)00040-7

Hall, R., Audley-Charles, M.G., Banner, F.T., Hidayat, S., Tobing, S.L., 1988. Late Palaeogene–Quaternary geology of Halmahera, Eastern Indonesia: initiation of a volcanic island arc. Journal of the Geological Society 145, 577–590. https://doi.org/10.1144/gsjgs.145.4.0577

Halmer, M.M., Schmincke, H.-U., Graf, H.-F., 2002. The annual volcanic gas input into the atmosphere, in particular into the stratosphere: a global data set for the past 100 years. Journal of

Volcanology and Geothermal Research 115, 511–528. https://doi.org/10.1016/S0377-0273(01)00318-3

Hamilton, W.B., 1979. Tectonics of the Indonesian region (No. 1078), Professional Paper. U.S. Govt. Print. Off.,. https://doi.org/10.3133/pp1078

Hawkesworth, C.J., Gallagher, K., Hergt, J.M., McDermott, F., 1993. Mantle and Slab Contributions in ARC Magmas. Annu. Rev. Earth Planet. Sci. 21, 175–204. https://doi.org/10.1146/annurev.ea.21.050193.001135

Hofmann, A.W., 1988. Chemical differentiation of the Earth: the relationship between mantle, continental crust, and oceanic crust. Earth and Planetary Science Letters 90, 297–314. https://doi.org/10.1016/0012-821X(88)90132-X

Keppler, H., 1996. Constraints from partitioning experiments on the composition of subduction-zone fluids. Nature 380, 237–240. https://doi.org/10.1038/380237a0

Kunrat, S., Bani, P., Haerani, N., Saing, U.B., Aiuppa, A., Syahbana, D.K., 2020. First gas and thermal measurements at the frequently erupting Gamalama volcano (Indonesia) reveal a hydrothermally dominated magmatic system. Journal of Volcanology and Geothermal Research 407, 107096. https://doi.org/10.1016/j.jvolgeores.2020.107096

Macpherson, C.G., Forrde, E.J., Hall, R., Thirlwall, M.F., 2003. Geochemical evolution of magmatism in an arc-arc collision: the Halmahera and Sangihe arcs, eastern Indonesia. Geological Society, London, Special Publications 219, 207–220. https://doi.org/10.1144/GSL.SP.2003.219.01.10

McCulloch, M.T., Gamble, J.A., 1991. Geochemical and geodynamical constraints on subduction zone magmatism. Earth and Planetary Science Letters 102, 358–374. https://doi.org/10.1016/0012-821X(91)90029-H

Morris, J.D., Jezek, P.A., Hart, S.R., Hill, J.B., 1983. The Halmahera Island Arc, Molucca Sea Collision Zone, Indonesia: A Geochemical Survey, in: The Tectonic and Geologic Evolution of Southeast

Asian Seas and Islands: Part 2. American Geophysical Union (AGU), pp. 373–387. https://doi.org/10.1029/GM027p0373

Moussallam, Y., Bani, P., Schipper, C.I., Cardona, C., Franco, L., Barnie, T., Amigo, Á., Curtis, A., Peters, N., Aiuppa, A., Giudice, G., Oppenheimer, C., 2018. Unrest at the Nevados de Chillán volcanic complex: a failed or yet to unfold magmatic eruption? Volcanica 1, 19–32. https://doi.org/10.30909/vol.01.01.1932

Ben Othman, D., White, W.M., Patchett, J., 1989. The geochemistry of marine sediments, island arc magma genesis, and crust-mantle recycling. Earth and Planetary Science Letters 94, 1–21. https://doi.org/10.1016/0012-821X(89)90079-4

Paris, R., Switzer, A.D., Belousova, M., Belousov, A., Ontowirjo, B., Whelley, P.L., Ulvrova, M., 2014. Volcanic tsunami: a review of source mechanisms, past events and hazards in Southeast Asia (Indonesia, Philippines, Papua New Guinea). Nat Hazards 70, 447–470. https://doi.org/10.1007/s11069-013-0822-8

Pin, C., Gannoun, A., Dupont, A., 2014. Rapid, simultaneous separation of Sr, Pb, and Nd by extraction chromatography prior to isotope ratios determination by TIMS and MC-ICP-MS. J. Anal. At. Spectrom. 29, 1858–1870. https://doi.org/10.1039/C4JA00169A

Plank, T., 2005. Constraints from Thorium/Lanthanum on Sediment Recycling at Subduction Zones and the Evolution of the Continents. Journal of Petrology 46, 921–944. https://doi.org/10.1093/petrology/egi005

Platt U, Stutz J., 2008. Differential optical absorption spectroscopy, principal and applications, Springer, 597 pp

Practical Application of Lead Triple Spiking for Correction of Instrumental Mass Discrimination, n.d. https://doi.org/10.1180/minmag.1998.62a.1.260

Saal, A.E., Hauri, E.H., Langmuir, C.H., Perfit, M.R., 2002. Vapour undersaturation in primitive mid-ocean-ridge basalt and the volatile content of Earth's upper mantle. Nature 419, 451–455. https://doi.org/10.1038/nature01073

Saing, U.B., Bani, P., Kristianto, 2014. Ibu volcano, a center of spectacular dacite dome growth and long-term continuous eruptive discharges. Journal of Volcanology and Geothermal Research 282, 36–42. https://doi.org/10.1016/j.jvolgeores.2014.06.011

Saing, U.B., Bani, P., Haerani, N., Aiuppa, A., Primulyana, S., Alfianti, H., Syahbana, D.K., Kristianto, 2020. First characterization of Gamkonora gas emission, North Maluku, East Indonesia. Bull Volcanol 82, 37. https://doi.org/10.1007/s00445-020-01375-7

Shinohara, H., 2005. A new technique to estimate volcanic gas composition: plume measurements with a portable multi-sensor system. Journal of Volcanology and Geothermal Research 143, 319–333. https://doi.org/10.1016/j.jvolgeores.2004.12.004

Siebert L, Simkin T, Kimberly P (2010) Volcanoes of the world, 3rd edn. Institution, Smithsonian

Stix, J., de Moor, J.M., 2018. Understanding and forecasting phreatic eruptions driven by magmatic degassing. Earth, Planets and Space 70, 83. https://doi.org/10.1186/s40623-018-0855-z

Symonds, R.B., Gerlach, T.M., Reed, M.H., 2001. Magmatic gas scrubbing: implications for volcano monitoring. Journal of Volcanology and Geothermal Research 108, 303–341. https://doi.org/10.1016/S0377-0273(00)00292-4

Turner, S., Hawkesworth, C., Rogers, N., Bartlett, J., Worthington, T., Hergt, J., Pearce, J., Smith, I., 1997. $^{238}U/^{230}Th$ disequilibria, magma petrogenesis, and flux rates beneath the depleted Tonga-Kermadec island arc. Geochimica et Cosmochimica Acta 61, 4855–4884. https://doi.org/10.1016/S0016-7037(97)00281-0

Zhang, Q., Guo, F., Zhao, L., Wu, Y., 2017. Geodynamics of divergent double subduction: 3-D numerical modeling of a Cenozoic example in the Molucca Sea region, Indonesia. Journal of Geophysical Research: Solid Earth 122, 3977–3998. https://doi.org/10.1002/2017JB013991

Voigt, S., Orphal, J., Bogumil, K., Burrows, J.P., 2001. The temperature dependence (203–293 K) of the absorption cross sections of O3 in the 230–850 nm region measured by Fourier-transform spectroscopy. Journal of Photochemistry and Photobiology A: Chemistry 143, 1–9. https://doi.org/10.1016/S1010-6030(01)00480-4

White, W.M., Albarède, F., Télouk, P., 2000. High-precision analysis of Pb isotope ratios by multi-collector ICP-MS. Chemical Geology 167, 257–270. https://doi.org/10.1016/S0009-2541(99)00182-5